Development 140, 2849 (2013) doi:10.1242/dev.099549

Reprogramming amacrine and photoreceptor progenitors into retinal ganglion cells by replaceing Neurod1 with Atoh7

Chai-An Mao[1], Jang-Hyeon Cho[1], Jing Wang[2], Zhiguang Gao[1], Ping Pan[1], Wen-Wei Tsai[1], Xiuqian Mu[3], Laura J. Frishman[2] and William H. Klein[1]

[1]Department of Biochemistry and Molecular Biology, The University of Texas MD Anderson Cancer Center, Houston, TX 77030, USA. [2]College of Optometry, University of Houston, Houston, TX 77204, USA. [3]Department of Ophthalmology/Ross Eye Institute, New York State Center of Excellence in Bioinformatics and Life Sciences, and SUNY Eye Institute, University at Buffalo, Buffalo, NY 14203, USA.

There was an error published in *Development* **140**, 541-551.

Author Xiuqian Mu was inadvertently omitted. Mu provided a mouse line for the study and also provided important conceptual input into the work.

The correct authors and affiliations are given above.

The authors apologise to readers for this mistake.

Development 140, 541-551 (2013) doi:10.1242/dev.085886

Reprogramming amacrine and photoreceptor progenitors into retinal ganglion cells by replacing *Neurod1* with *Atoh7*

Chai-An Mao[1,*], Jang-Hyeon Cho[1], Jing Wang[2], Zhiguang Gao[1], Ping Pan[1], Wen-Wei Tsai[1,‡], Laura J. Frishman[2] and William H. Klein[1,*]

SUMMARY

The specification of the seven retinal cell types from a common pool of retina progenitor cells (RPCs) involves complex interactions between the intrinsic program and the environment. The proneural basic helix-loop-helix (bHLH) transcriptional regulators are key components for the intrinsic programming of RPCs and are essential for the formation of the diverse retinal cell types. However, the extent to which an RPC can re-adjust its inherent program and the mechanisms through which the expression of a particular bHLH factor influences RPC fate is unclear. Previously, we have shown that *Neurod1* inserted into the *Atoh7* locus activates the retinal ganglion cell (RGC) program in *Atoh7*-expressing RPCs but not in *Neurod1*-expressing RPCs, suggesting that *Atoh7*-expressing RPCs are not able to adopt the cell fate determined by *Neurod1*, but rather are pre-programmed to produce RGCs. Here, we show that *Neurod1*-expressing RPCs, which are destined to produce amacrine and photoreceptor cells, can be re-programmed into RGCs when *Atoh7* is inserted into the *Neurod1* locus. These results suggest that *Atoh7* acts dominantly to convert a RPC subpopulation not destined for an RGC fate to adopt that fate. Thus, *Atoh7*-expressing and *Neurod1*-expressing RPCs are intrinsically different in their behavior. Additionally, ChIP-Seq analysis identified an Atoh7-dependent enhancer within the intronic region of *Nrxn3*. The enhancer recognized and used Atoh7 in the developing retina to regulate expression of *Nrxn3*, but could be forced to use Neurod1 when placed in a different regulatory context. The results indicate that Atoh7 and Neurod1 activate distinct sets of genes *in vivo*, despite their common DNA-binding element.

KEY WORDS: Retinal ganglion cells, Retinal progenitor cells, bHLH genes, Atoh7/Math5, Neurod1, Mouse

INTRODUCTION

Over the course of development, vertebrate retina progenitor cells (RPCs) acquire distinct competency states for cell fate specification by continuously adjusting their intrinsic properties in response to a dynamically changing local environment (Livesey and Cepko, 2001; Agathocleous and Harris, 2009; Wallace, 2011). Through this intricate but vaguely understood process, the seven retinal cell types are produced in an overlapping spatiotemporal sequence between embryonic day 11 (E11) and postnatal day 21 (P21) (Rodieck, 1998; Wallace, 2011).

The proneural basic helix-loop-helix (bHLH) family of transcriptional factors has special significance in establishing the intrinsic properties of RPCs. Acting singly or in combination, proneural bHLH factors direct the commitment and formation of the diverse retinal cell types (Perron and Harris, 2000; Ohsawa and Kageyama, 2008). For example, *Atoh7*, the mouse ortholog of *Drosophila Atonal*, is first expressed around E11 in a subset of RPCs and is essential for establishing the competency state for retinal ganglion cell (RGC) fate (Brown et al., 1998; Yang et al., 2003; Brzezinski et al., 2012). RGC differentiation soon begins in a subpopulation of *Atoh7*-expressing RPCs. Genetic ablation of *Atoh7* results in ~95% loss of RGC formation (Fig. 1A) (Brown et al., 2001; Wang et al., 2001). At the same time, other proneural bHLH factors, most notably *Neurod1*, *Math3*, *Mash1* and *Ptf1a*, are detected in distinct subpopulations of RPCs and are required for establishing non-RGC cell fates (Vetter and Brown, 2001; Akagi et al., 2004; Hatakeyama and Kageyama, 2004; Le et al., 2006; Ohsawa and Kageyama, 2008; Trimarchi et al., 2008). Deletion of *Neuord1* leads to the loss of the M-cone cell type (Fig. 1B) (Liu et al., 2008), and deletion of *Ptf1a* in a subpopulation of RPCs results in a loss of horizontal and amacrine cells (Fujitani et al., 2006). In addition, more complex cross-regulatory interactions between bHLH genes are often required for establishing the retinal cell types. Deletion of *Neurod1* and *Math3* together leads to an absence of amacrine cells (Inoue et al., 2002), and deletion of *Math3* and *Mash1* regulates the genesis of bipolar cells (Hatakeyama and Kageyama, 2004). Proneural bHLH genes are also involved in the specification of specific subtypes of retinal cells. *Bhlhb5*, a member of the oligo subfamily of bHLH factors, is required for the formation of type 2 off-cone bipolar cells and selective GABAergic amacrine cells (Feng et al., 2006). In postnatal retinas, *Neurod2* is expressed in subsets of RPCs, Dab+ AII amacrine cells (AII ACs), RGCs and cone bipolar cells. Loss of *Neurod2* leads to decreased formation of AII ACs (Cherry et al., 2011), yet misexpression of *Neurod2* induces the production of amacrine cells and RGCs. *Neurod6* is detected in nGnG amacrine cells, a newly discovered subclass of amacrine cell subtypes, and is sufficient to promote the formation of this amacrine cell subclass (Kay et al., 2011; Cherry et al., 2011).

The mosaic spatiotemporal pattern of the proneural bHLH factors in developing retinas, which seemingly mirrors the competency state in the RPCs, raises the issue of how these bHLH factors function independently and synergistically with each other and with non-bHLH factors to regulate the competency state of RPCs. The predominant view of cell fate determination in the developing retina is that the interspersed spatiotemporal expression

[1]Department of Biochemistry and Molecular Biology, The University of Texas MD Anderson Cancer Center, Houston, TX 77030, USA. [2]College of Optometry, University of Houston, Houston, TX 77204, USA.

[‡]Present address: The Salk Institute, San Diego, CA 92186, USA
*Authors for correspondence (cmao@mdanderson.org; whklein@mdanderson.org)

Accepted 14 November 2012

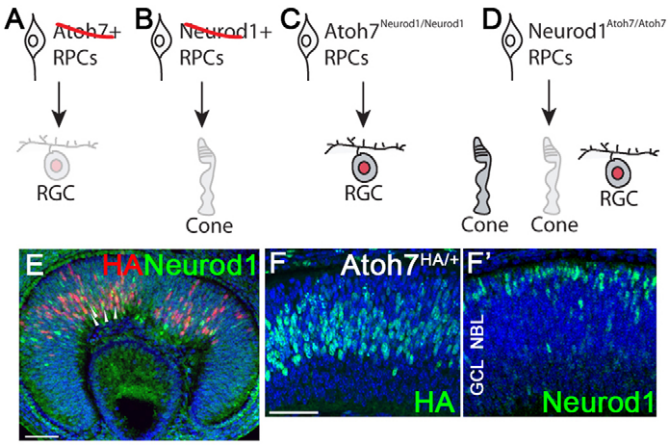

Fig. 1. Phenotypic consequences of loss and gain of *Atoh7* and *Neurod1* function and their mosaic expression patterns in interspersed RPCs during retinogenesis. (**A**) Loss of *Atoh7* leads to ~95% loss of RGCs owing to failed RGC specification during embryonic stages. (**B**) Loss of *Neurod1* leads to loss of M-cones during retinogenesis. (**C**) Replacing *Atoh7* with *Neurod1* leads to ~40% recovery of RGC formation during developmental stages. (**D**) Possible outcomes when *Neurod1* is replaced with *Atoh7*: (left) *Atoh7* compensates for the function of *Neurod1* in forming M-cones; (middle) no function; and (right) *Atoh7* specifies RGCs in *Neurod1*-expressing RPCs. (**E-F′**) $Atoh7^{HA/+}$ retinas stained with anti-HA and anti-Neurod1 antibodies at E12.5 (E) and E14.5 (F,F′). Scale bars: 50 μm.

patterns of *Atoh7*, *Neurod1* and other factors arise stochastically. This implies that all RPCs have equivalent developmental potential. The onset of bHLH gene expression relies on the downregulation of Notch signaling in a subset of RPCs (Wallace, 2011). Once established, each subset of RPCs is biased to give rise to distinct types of neurons depending on the bHLH factors they express (Agathocleous and Harris, 2009; Wallace, 2011).

Previously, we tested whether replacing one bHLH gene with another could redirect RPCs from one cell fate into another (Mao et al., 2008b). We inserted *Neurod1* into the *Atoh7* locus and showed that *Neurod1* replaced the function of *Atoh7* in specifying RGC fate. The results suggested that *Atoh7*-expressing RPCs are largely programmed by intrinsic mechanisms that are not solely dependent on a specific proneural bHLH gene (Fig. 1C). In the same study, we also showed that *Math3* did not compensate for the loss of *Atoh7*. We thus concluded that *Neurod1* and *Atoh7* share similar gene targets in the developing retina, whereas *Math3* does not. Despite the fact the *Neurod1* normally functions in RPCs destined for amacrine cell and M-cone cell fate, it adjusts and integrates into the foreign environment of RPCs destined for a RGC fate. Notably, *Neurod1*-null retinas produce the full complement of RGCs, indicating that *Neurod1*-expressing RPCs play little if any role in RGC differentiation (Liu et al., 2000; Pennesi et al., 2003; Liu et al., 2008). Hence, *Neurod1*-expressing RPCs, unlike *Atoh7*-expressing RPCs, are not intrinsically programmed for RGC formation. These results argue against the view that RPCs are equally potent in their potential to generate multiple cell types at the same developmental time. If this view is correct, then *replacing Atoh7* with *Neurod1* would be expected to *reprogram Atoh7*-expressing RPCs into amacrine cells or M-cone cells, which they do not do.

In the present study, we performed the converse experiment by inserting *Atoh7* into the *Neurod1* locus. Our aim was to determine which model most correctly describes the behavior of *Neurod1*-expressing RPCs: (1) *Atoh7* compensates for the loss of *Neurod1* to restore M-cone cells; (2) *Atoh7* is not tolerated in *Neurod1*-expressing RPCs and cannot compensate for the absence of *Neurod1*; or (3) *Atoh7* functions dominantly as a master regulator for RGC competency (Fig. 1D).

The experiments described below show that *Atoh7* alone is sufficient to redirect an RPC destined to form an amacrine/M-cone cell fate to an RGC fate, and that early arising *Neurod1*-expressing RPCs are inherently programmed to produce RGCs, although they require *Atoh7* to do so. Together with our previous results (Mao et al., 2008b), we propose that, in early retinogenesis, most RPCs have the developmental potential to differentiate into RGCs. Although the extrinsic environment plays a role in this process, subtle intrinsic differences must exist among different RPC subpopulations that can be overcome by the expression of *Atoh7*. In addition, we identify a bona fide Atoh7-binding enhancer in the intron 3 region of neurexin III (*Nrxn3*). We demonstrate that this enhancer is bound and used by Atoh7 but not by Neurod1 in the developing retina. By placing the *Nrxn3* enhancer next to a basal promoter, we show that the enhancer is recognized by both Atoh7 and Neurod1. These results suggest that the *Nrxn3* enhancer element is selectively used by similar factors in a context-dependent manner, thus providing a mechanism for determining the specialized functions that exist among multiple proneural bHLH factors.

MATERIALS AND METHODS

Gene targeting, transgenic animals and animal breeding

The targeting vector (Fig. 2A) was constructed by standard molecular biology techniques using PCR-amplified genomic DNA fragments from the *Neurod1* locus as homologous arms. The *Atoh7*-coding sequence was fused to sequences encoding three copies of the hemagglutinin epitope YPYDVPDYA (HA-tag), and inserted after the PGK-Neo cassette, which was flanked by two loxC2 sites. Gene targeting was conducted as described previously (Mao et al., 2008b). Two targeted ES cell lines were used to generate $Neurod1^{FNeoAtoh7HA3/+}$ mice. The $Neurod1^{FNeoAtoh7HA3/+}$ line was subsequently bred to a germline *CMV-Cre* line to generate the $Neurod1^{Atoh7HA3/+}$ line, which appeared normal. The knock-in allele was distinguished using PCR with primers B2 (5′-GTGTGCATTTCT-GTAGGATTAGGG-3′), B3 (5′-GCTCTCGCTGTATGATTTGGTCATG-3′) and M51 (5′-GACACAGACGGAGCGACTCACGTG-3′) (Fig. 2B). To generate $Nrxn^{3A7E}$*-HSP68LacZ* transgenic mouse lines, we fused a 489 bp sequence (chr12: 90280064-90280552) expanded from the 326 bp Atoh7-bound sequence-tag in *Nrxn3*, named $Nrxn3^{A7E}$, to a *HSP68pro-lacZ* reporter (Kothary et al., 1989). This construct was used for pronuclear injection to generate transgenic mice. $Atoh7^{G/G}$ mice were as described by Wang et al. (Wang et al., 2001); $Atoh7^{HA/HA}$ mice were as described by Fu et al. (Fu et al., 2009). All animal procedures followed the US Public Health Service Policy on Humane Care and Use of Laboratory Animals, and were approved by the Institutional Animal Care and Use Committee at The University of Texas MD Anderson Cancer Center.

Immunohistochemistry and *in situ* hybridization

Mouse embryos and eyes dissected from embryos or adults were fixed, embedded in paraffin or OCT, and sectioned into 12 μm or 20 μm slices for immunohistochemistry. The sections were placed in a microwave oven at 600 W in 10 mM sodium citrate for 15 minutes to expose the antigen epitopes. For indirect immunofluorescence, a tyromide signal amplification kit (PerkinElmer) was used for Neurod1 and Pou4f2 to optimize signal intensity. The primary antibodies were anti-β-galactosidase (MP Biomedicals, 1:2000), anti-BrdU (Upstate, 1:10), anti-Isl1 (DSHB, 1:250), anti-HA (Cell Signaling, 1:500), anti-NF-L (Invitrogen, 1:500), anti-Opsin(R/G) (Chemicon, 1:500), anti-Pou4f1/Brn3a (Chemicon, 1:150), anti-Pou4f2/Brn3b (Santa Cruz, 1:100), anti-SMI32 (Covance, 1:400) and

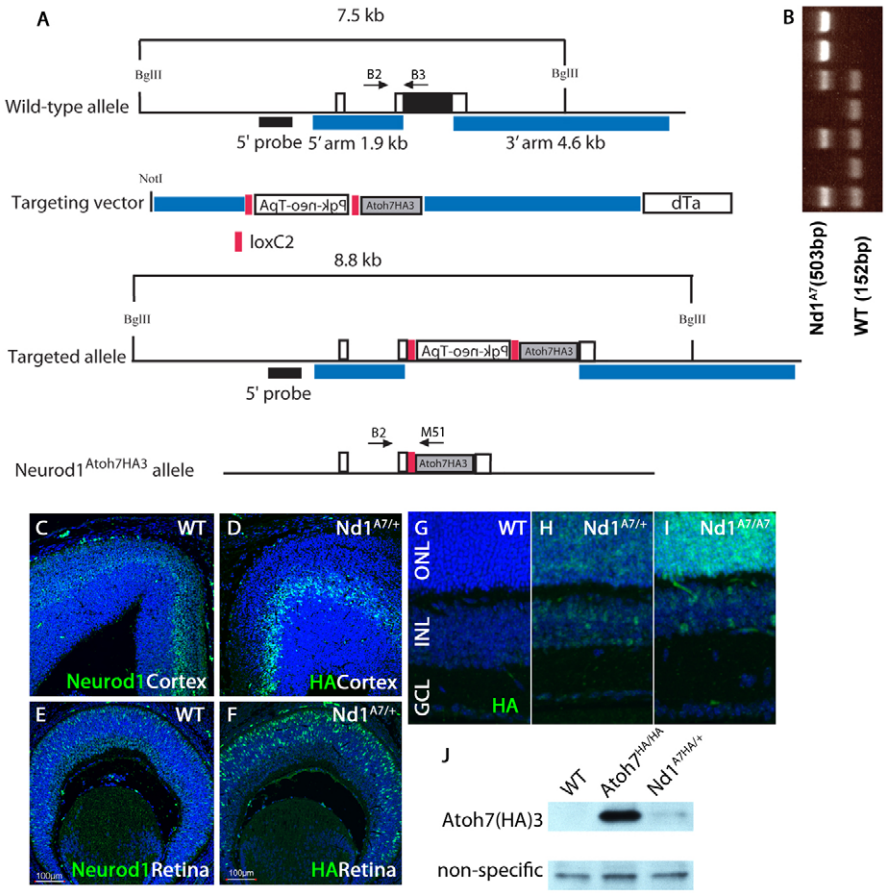

Fig. 2. Replacing endogenous *Neurod1* with *Atoh7HA3*. (**A**) Genome structure for *Neurod1*, the targeting construct and the predicted *Atoh7HA3* knock-in allele. The coding region of *Neurod1* is depicted as a black box. The blue bars underneath indicate the two arms for the targeting construct. Red boxes depict loxC2 sites. *Atoh7HA3* is indicated as gray box. (**B**) Representative PCR analysis using B2, B3 and M51 to distinguish wild-type and *Neurod*^{Atoh7HA} (Nd1^{A7}) alleles from tail DNA. (**C-F**) Mis-expression of *Atoh7HA3* from the *Neurod1* locus. Sections of cortex (C,D) and retina (E,F) from E14.5 wild-type (C,E) and *Nd1*$^{A7/+}$ (D,F) embryos were immunostained with anti-Neurod1 (C,E) or anti-HA (D,F) antibodies. (**G-I**) Adult retinal sections of wild-type (G), *Neurod1*$^{Atoh7HA/+}$ (H) and *Neurod1*$^{Atoh7HA/Atoh7HA}$ (I) were stained with anti-HA antibody. (**J**) Western analysis of Atoh7HA3 protein expression from E14.5 retinas of *Atoh7*$^{HA/HA}$ and *Neurod1*$^{Atoh7HA/+}$ mice. The non-specific bands were used as loading controls. Scale bars: 100 μm.

anti-Ngn2 (R&D Systems, 1:50). Alexa-conjugated and HRP-conjugated secondary antibodies were from Invitrogen and Jackson ImmunoResearch. To detect RGC axons and to estimate RGC number, anti-NF-L and anti-Pou4f2/Brn3b antibodies were used to stain flat-mounted retinas (Mao et al., 2008a). Images were captured and analyzed using an Olympus Fluoview 1000 confocal microscope. *In situ* hybridization was performed as described by Mao et al. (Mao et al., 2008b).

RGC axon tracing

Cholera toxin subunit (CTB; 2 μl) conjugated with either Alexa-488 or -594 (1 mg/ml, Invitrogen) was injected into the vitreous using a 36-gauge NanoFil system (World Precision Instruments). Two days later, animals were anesthetized and sacrificed with perfusion using 4% PFA. Whole brains were dissected and post-fixed with 4% PFA.

Western analysis

Whole cell lysate (20 μg) from E14.5 retinas were resolved on 10% SDS-PAGE gels (Bio-Rad) and transferred onto PVDF a membrane. Primary antibody against HA epitope tag (Abcam) and HRP-conjugated secondary antibody were applied to the membrane. Proteins were detected using ECL substrate (Amersham Biosciences). Protein expression was quantified using ImageJ (http://rsb.info.nih.gov/ij/docs/menus/analyze.html#gels). The intensity ratio between Neurod1$^{Atoh7(HA)/+}$ and Atoh7$^{HA/HA}$ bands was adjusted by the ratio of the total number of Neurod1-expressing and Atoh7-expressing RPCs counted at E14.5 to quantify the relative level of Atoh7HA on the per cell basis between the Neurod1^{Atoh7} and Atoh7^{HA} alleles.

Transmission electron microscopy

Enucleated eyes with the optic nerve were fixed with 3% glutaraldehyde and 2% paraformaldehyde in 0.1 M sodium cacodylate (pH 7.5) for 1 hour at room temperature. Samples were washed and treated with 0.1% cacodylate-buffered tannic acid, post-fixed with 1% osmium tetroxide, strained *en bloc* with 1% uranyl acetate and dehydrated with an ethanol gradient series. The samples were embedded in epon and sectioned with an LKB ultracut microtome. Sections were examined using a JEM 1010 TEM (JEOL).

Scotopic electroretinograms (ERG) recordings and data analysis

Mice were dark-adapted overnight and all preparations for recording were performed under dim red illumination (λ>650 nm) (Saszik et al., 2002). Animals were anesthetized with ketamine (70 mg/kg) and xylazine (7 mg/kg), and anesthesia was maintained with subcutaneous injections of ketamine (20 mg/kg) and xylazine (1 mg/kg) every 20-30 minutes. The head of each animal was fixed in a metal head holder that also served as the electrical ground. Pupils were fully dilated to 3 mm in diameter with topical atropine (0.5%) and phenylephrine (2.5%). Body temperature was monitored and maintained at 37°C with a thermostatically controlled electrically heated blanket (CWE). Full-field flash ERGs were recorded using DTL fiber electrodes placed across the center of the cornea of the tested eye and the fellow eye, which served as the reference. The cornea of the tested eye was covered with a contact lens heat-formed from clear film (ACLAR film). The non-tested eye was covered with a black plastic (PVC) contact lens and a black aluminum foil cap that covered both the eye and the skull to block any scattered light. Stimuli were provided from LEDs (λ_{max}=462 nm) at a range of time-integrated flash luminances (stimulus strengths) from −6.2 to 3.0 log scotopic troland seconds (sc td-s). The inter-flash interval was adjusted to allow the ERG response to return to baseline between stimuli. For data analysis, A-wave amplitudes were measured on the leading edge of the wave, at a fixed time (6 ms) after the brief flash. After oscillatory potentials (>50 Hz) were removed, b-wave amplitudes were measured between the a-wave trough and b-wave peak, and also at the peak of pSTR and b-wave, 110 ms after the brief flash. nSTR amplitude was measured at 200 ms after the flash. B-waves were also measured from the trough of the a-wave to the peak of the b-wave. Repeated-measures ANOVA (SPSS) was performed to compare amplitudes of the stimulus response functions across all groups, and between pairs of groups.

Chromatin immunoprecipitation

Twenty E14 *Atoh7*$^{HA/HA}$ retinas were used for ChIP reactions following the procedure described by Tsai et al. (Tsai et al., 2010) to produce fragmented chromatin lysate. The fragmented, precleared chromatin lysate was incubated overnight with anti-HA (Cell Signaling), Neurod1 (Santa Cruz) or normal goat IgG (Santa Cruz). To analyze specific Atoh7HA-bound DNA, qPCR was conducted in a 7500 FAST ABI instrument. Sequences for PCR primers used were Tbr1f (5′-CAGCCCCAGTCGCTACATGG-3′), Tbr1r (5′-GCCCTGCGGCGAAGAGTTG-3′), Nrxn3f (5′-CAGGGAGAGTCATAAGGAGAAAA-3′) and Nrxn3r (5′-CAGCACATGTCATCCTAACACTT-3′). Total RNA was collected from E14.5 retinas using Trizol reagent (Invitrogen). RNAs were reversed transcribed using the SuperScript First-Strand Synthesis System (Invitrogen) following the manufacturer's instructions. For quantitative reverse transcriptase-PCR analysis, cDNAs were amplified using SYBR green PCR master mix (Applied Biosystems). The relative expression levels were normalized to that of GAPDH and calculated using the comparative C_t method (7500 Fast Real-time PCR systems SDS software, Applied Biosystems). DNA sequences of PCR primers were GAPDH-f (5′-AGGTCGGTGTGAACGGATTTG-3′), GAPDH-r (5′-TGTAGACCATGTAGTTGAGGTCA-3′) Nrxn3-f (5′-TTGGCACCATTGATGACCTG-3′) and Nrxn3-r (5′-CTTCAATAGCGGAGATGGCA-3′).

RESULTS

Expression of *Atoh7* and *Neurod1* in early embryonic retinas mirrors the competency state of distinct subsets of RPCs

To compare the spatial and temporal expression patterns of *Atoh7* and *Neurod1* in early embryonic retinas, we used anti-HA and anti-Neurod1 antibodies to label retinas of E12.5 *Atoh7*$^{HA/+}$ embryos. *Atoh7*^{HA} is a knock-in allele in which the *Atoh7*-coding sequence is fused in-frame with three copies of haemagglutinin (HA) (Fu et al., 2009). Atoh7-HA labeling was detected in the central part of retina where retinogenesis begins (Fig. 1E). By contrast, Neurod1 labeling was detected weakly in a slightly wider area where naïve RPCs reside (Fig. 1E). Only a few Neurod1-positive RPCs also expressed Atoh7-HA (Fig. 1E, arrowheads). At E14.5, Atoh7-HA expression was detected in RPCs throughout neural blast layer (NBL) (Fig. 1F), whereas Neurod1 was weakly expressed in the NBL, and its expression tended to cluster closer to the area where the presumptive photoreceptor cells reside (Fig. 1F′). The total number of RPCs expressing Atoh7-HA was about one and a half fold higher than Neurod1-expressing RPCs at E12 and twofold higher at E14.5 (cells/field: 155.7±5.9 versus 78.3±10.1; n=3, P<0.01).

Neurod1^{Atoh7} mimics endogenous *Neurod1* expression patterns and cannot rescue phenotypic defects seen in *Neurod1*$^{-/-}$ mice

Atoh7-expressing and *Neurod1*-expressing RPCs are interspersed at similar developmental times yet they are required for the formation of different retinal neurons. To determine how these distinct subpopulations of RPCs responded to the activity of *Atoh7*, we have generated a *Neurod1*$^{Atoh7HA/+}$ allele by gene targeting (Fig. 2A,B) (referred to as Nd1^{A7} in the figures). We first determine whether the *Neurod1*$^{Atoh7HA/+}$ allele was expressed in a pattern that was similar to that of endogenous *Neurod1*. At E14.5, *Neurod1*$^{Atoh7HA/+}$ was weakly expressed throughout the retina and in the cortex, similar to endogenous *Neurod1* expression (Fig. 2C-F). In the mature retina, Neurod1 was also weakly expressed in both outer nuclear layer (ONL) and inner nuclear layer (INL). In the adult *Neurod1*$^{Atoh7HA/+}$ retina, Atoh7-HA was also detectable in ONL and INL in a dose-dependent manner (Fig. 2G-I). We observed that Atoh7-HA expression in the *Neurod1*$^{Atoh7HA/+}$ allele was much weaker on a per cell basis compared with that in the *Atoh7*$^{HA/+}$ allele. We compared expression levels by western analysis, and found a 10-fold difference in Atoh7-HA expression between Atoh7$^{HA/+}$ and Neurod1$^{Atoh7HA/+}$ alleles (Fig. 2J).

Neurod1 is expressed in many regions in the central and peripheral nervous systems during development. A number of behavioral abnormalities associated with *Neurod1*-deficient mice have been reported, including head tilting and circling (Liu et al., 2000; Pennesi et al., 2003) that are due to defects in the cerebellum and inner ear. We found that all *Neurod1*$^{Atoh7HA/Atoh7HA}$ mice displayed this balancing defect. Examination of the cerebellum of *Neurod1*$^{Atoh7HA/Atoh7HA}$ mice showed that *Neurod1*$^{Atoh7HA/Atoh7HA}$ cerebellum has similar defects as found in Neurod1$^{-/-}$ mice (data not shown), suggesting that *Atoh7-HA*, although expressed in identical regions to *Neurod1*, could not rescue the function of *Neurod1* in cerebellum and inner ear development. In addition, in developing retinas, Neurod1 activates the expression of thyroid hormone receptor β2 (*Trb2*; *Thrb* – Mouse Genome Informatics) to regulate the formation of M-opsin in a dorsal-ventral gradient manner (Liu et al., 2008). In *Neurod1*$^{-/-}$ retinas, all cone photoreceptors express short-wavelength (S) opsin. We thus examined the S-opsin expression in *Neurod1*$^{Atoh7HA/Atoh7HA}$ retinas and found that most of the cone cells in the dorsal retina expressed S-opsin (supplementary material Fig S1A-D), suggesting that *Atoh7-HA* cannot rescue the ability of *Neurod1* to regulate the formation of M-cone cells.

Increased RGCs production in *Neurod1*$^{Atoh7HA/Atoh7HA}$ retinas

Atoh7 is required for the formation of RGCs in mice and humans (Wang et al., 2001, Brown et al., 2001, Ghiasvand et al., 2011). Hence, we determined whether *Neurod1*$^{Atoh7HA/Atoh7HA}$ retinas produced more RGCs than wild-type retinas. In P30 mice, immunostaining flat-mounted retinas with an anti-neurofilament light chain (NF-L) antibody showed that all *Neurod1*$^{Atoh7HA/Atoh7HA}$ retinas analyzed had a significantly higher density of RGC axon bundles compared with those of wild-type retinas (Fig. 3A,B). To determine how many more RGCs were generated in *Neurod1*$^{Atoh7HA/Atoh7HA}$ retinas, we immunostained P30 retinal sections with anti-Pou4f1/Brn3a antibody, and observed ~20% more Pou4f1-positive RGCs in *Neurod1*$^{Atoh7HA/Atoh7HA}$ retinas than in wild-type controls (Fig. 3C,D, arrowheads). Interestingly, we detected displaced retinal ganglion cells (dRGCs) expressing Pou4f1 in the innermost region of the INL in *Neurod1*$^{Atoh7HA/Atoh7HA}$ retinas (Fig. 3E). These Pou4f1-expressing dRGCs often expressed SMI32, an RGC subtype marker that also labeled RGC axons (Fig. 3E, arrowheads), whereas we rarely detect expression of these genes in INL of wild-type retinas. The Pou4f1-positive dRGCs found in the INL of *Neurod1*$^{Atoh7HA/Atoh7HA}$ retinas could arise during development by a failure to migrate to the ganglion cell layer (GCL) as a consequence of improper spatiotemporal specification. Alternatively, some *Neurod1*-expressing amacrine cells could be converting to RGCs as *Atoh7* is expressed under the control of *Neurod1*.

We conducted birthdating analysis to track when these cells were born and found that Pou4f1-expressing dRGCs were BrdU positive when BrdU was injected at E17.5 (Fig. 3F, arrowhead), suggesting that these dRGCs were born during late embryonic development. Whether they were born as RGCs and failed to migrate to the GCL, or born as non-RGC types and converted to RGCs was unclear.

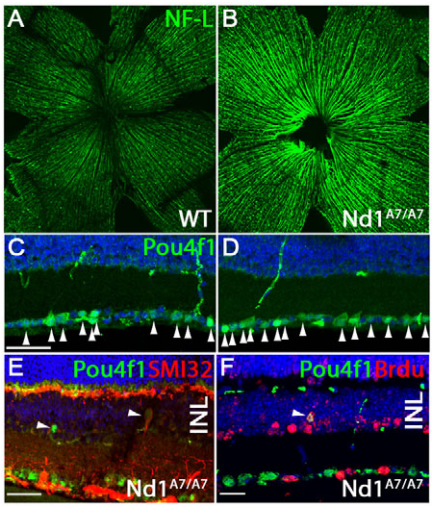

Fig. 3. *Neurod1*$^{Atoh7HA/Atoh7HA}$ mice produce more RGCs and displaced RGCs (dRGCs) in the INL. (**A**,**B**) Retinal flat-mount immunostaining using anti-NF-L antibody on wild-type (A) and *Neurod1*$^{Atoh7HA/Atoh7HA}$ (B) retinas. (**C**,**D**) Immunostaining using anti-Pou4f1 antibody on P30 (C) wild-type and (D) *Neurod1*$^{Atoh7HA/Atoh7HA}$ retinal sections. (**E**) Immunostaining using anti-Pou4f1 and anti-SMI32 antibodies on P30 *Neurod1*$^{Atoh7HA/Atoh7HA}$ retinas. (**F**) Birth-dating analysis of Pou4f1-positive dRGCs in *Neurod1*$^{Atoh7HA/Atoh7HA}$ retinas when BrdU was injected at E17.5 and retinas dissected at P20. Retinal section was co-labeled with anti-Pou4f1 and anti-BrdU antibodies. INL, inner nuclear layer. Scale bars: 40 μm in C,E,F.

Partial restoration of optic nerves and RGC axons in *Atoh7*$^{G/G}$*:Neurod1*$^{Atoh7HA/Atoh7HA}$ mice

In the presence of endogenous *Atoh7*, the *Neurod1*^{Atoh7HA} allele resulted in 20% more RGCs and RGC axons. We expected that in the absence of *Atoh7*, the *Neurod1*^{Atoh7HA} would lead to a restoration of RGCs and possibly optic nerves, the major tissues affected in *Atoh7*$^{G/G}$ mice (Wang et al., 2001). To determine whether *Neurod1*$^{Atoh7HA/Atoh7HA}$-induced RGCs could rescue the optical nerve defect, we crossed *Neurod1*$^{Atoh7HA/Atoh7HA}$ mice with *Atoh7*$^{G/G}$ mice and isolated eyes from adult *Atoh7*$^{G/G}$*:Neurod1*$^{Atoh7HA/Atoh7HA}$ mice. Notably, we found the dissected eyes attached to partially developed optic nerves. Low magnification transmission electron microscopy (TEM) revealed that their diameters were 30% to 40% of those in wild-type mice (Fig. 4A,B). We examined optic nerve ultrastructure using higher magnification TEM, and observed that RGC axons were ensheathed with a well-organized and compact myelinated layer (Fig. 4C,D). The presence of optic nerves in *Atoh7*$^{G/G}$*:Neurod1*$^{Atoh7HA/Atoh7HA}$ mice suggested that RGC axons were forming, fasciculating and extending into the optic disk. We performed retinal flat-mount immunostaining from P30 mice with anti-NF-L antibody and observed that *Atoh7*$^{G/G}$*:Neurod1*$^{Atoh7HA/Atoh7HA}$ retinas had significant numbers of well-bundled RGC axons projecting towards the optic disk (Fig. 4E,F). To measure the number of RGCs that were generated in *Atoh7*$^{G/G}$*:Neurod1*$^{Atoh7HA/Atoh7HA}$ retinas, we performed flat-mount immunostaining on P30 retinas with anti-Pou4f2/Brn3b antibody and found that *Atoh7*$^{G/G}$*:Neurod1*$^{Atoh7HA/Atoh7HA}$ retinas had about 25% of the number of RGCs of wild-type retinas (cells/field: 155.25±9.11 versus 39.75±5.90; n=4, P<0.01). Furthermore, RGCs were generated evenly across the dorsal-ventral and the nasal-temporal axes within *Atoh7*$^{G/G}$*:Neurod1*$^{Atoh7HA/Atoh7HA}$ retinas.

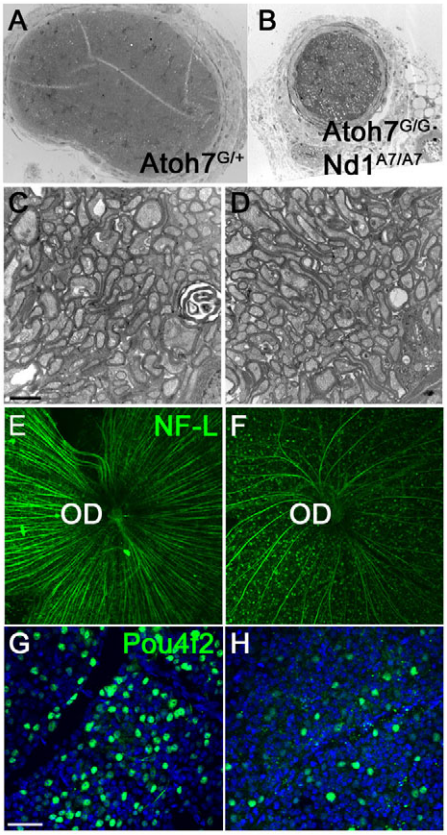

Fig. 4. Partial restoration of RGCs and optic nerves in *Atoh7*$^{G/G}$*:Neurod1*$^{Atoh7HA/Atoh7HA}$ retinas. (**A-D**) Transmission electron microscopy analysis of optic nerve cross-sections. C and D are at higher magnification. (**E-H**) Retinal flat-mount immunostaining using anti-NF-L (E,F) and anti-Pou4f2 (G,H). (A,C,E,F) Wild-type and (B,D,F,H) *Atoh7*$^{G/G}$*:Neurod1*$^{Atoh7HA/Atoh7HA}$ retinas. OD, optic disk. Scale bars: 2 μm in C; 50 μm in G.

Expression of RGC genes in embryonic retinas of *Atoh7*$^{G/G}$*:Neurod1*^{Atoh7HA} mice

RGC differentiation begins at E12.5 when *Isl1* and *Pou4f2/Brn3b* are first expressed in naïve RGCs (Gan et al., 1999; Elshatory et al., 2007; Mu et al., 2008). To determine when *Atoh7*$^{G/G}$*:Neurod1*$^{Atoh7HA/Atoh7HA}$ retinas first generate RGCs, we used an anti-Isl1 antibody to determine its expression pattern in E13 retinas. We found that *Atoh7*$^{G/G}$*:Neurod1*$^{Atoh7HA/Ahot7HA}$ retinas restored 28% of Isl1-positive RGCs compared with wild-type retinas (Fig. 5A,D), whereas *Neurod1*$^{Atoh7HA/Atoh7HA}$ retinas had 30% more Isl1-positive RGCs compared with wild-type retinas (Fig. 5A,B). Similarly, immunostaining using anti-Pou4f2 antibody also showed that *Atoh7*$^{G/G}$*:Neurod1*$^{Atoh7HA/Atoh7HA}$ retinas produce more RGCs compared with Atoh7$^{G/G}$ retina (Fig. 5F,G), and restored 26% of RGCs compared with wild-type retinas (Fig. 5E,G). These results suggested that *Neurod1*-expressing RPCs, although destine to produce amacrine cells and cone cells during development, were inherently capable of being reprogrammed to produce RGCs when *Atoh7* was ectopically expressed.

Atoh7$^{G/G}$*:Neurod1*$^{Atoh7/Atoh7}$-induced RGCs project to lateral geniculate nucleus and superior colliculus

The lateral geniculate nucleus (LGN) and superior colliculus (SC) are two of the major targets of the RGC axons in the brain. The

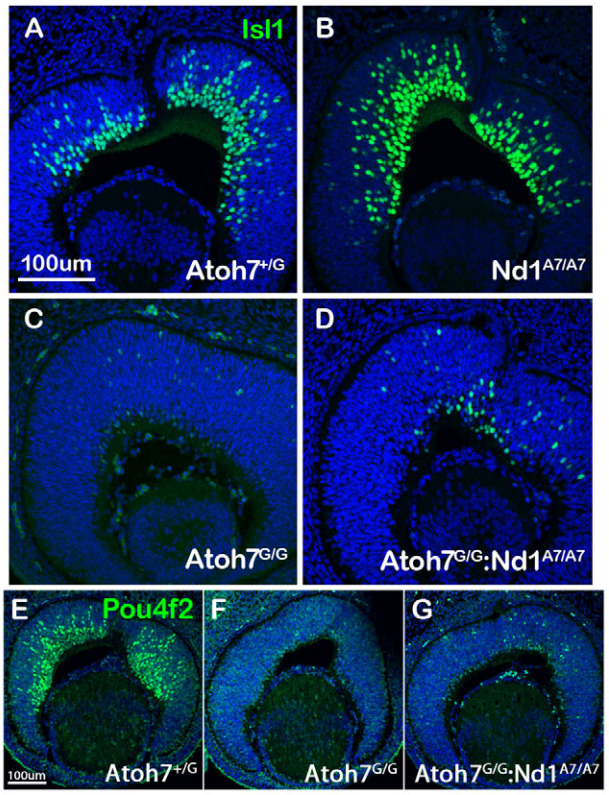

Fig. 5. Activation of early expressed RGC genes in *Atoh7*$^{G/G}$:*Neurod1*$^{Atoh7HA/Atoh7HA}$ retinas. (**A-G**) Immunostaining of retinas from E13 embryos with anti-Isl1 antibody (A-D) on (A) *Atoh7*$^{G/+}$, (B) *Neurod1*$^{Atoh7HA/Atoh7HA}$, (C) *Atoh7*$^{G/G}$ and (D) *Atoh7*$^{G/G}$:*Neurod1*$^{Atoh7HA/Atoh7HA}$ retinal sections, and with anti-Pou4f2/Brn3b antibody (E-G) on (E) *Atoh7*$^{G/+}$, (F) *Atoh7*$^{G/G}$ and (G) *Atoh7*$^{G/G}$:*Neurod1*$^{Atoh7HA/Atoh7HA}$ retinal sections. Scale bars: 100 μm.

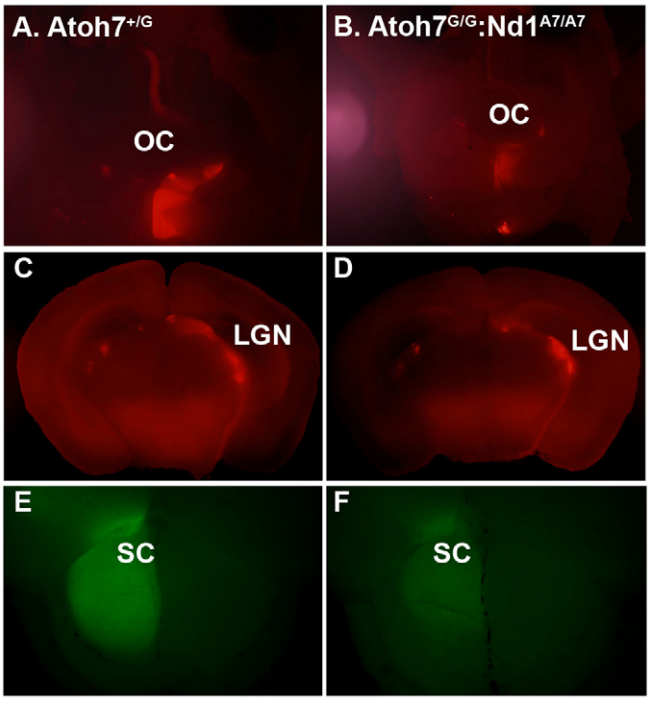

Fig. 6. RGC axon targeting in the brain. (**A**,**B**) Dorsal view RGC axon tracing in the brain of mice whose left eyes were injected with CTB-594. The RGC axons travel through the optic chiasm (OC) to the right side of the brain in *Atoh7*$^{+/G}$ mice (A) and *Atoh7*$^{G/G}$:*Neurod1*$^{Atoh7/Atoh7}$ mice (B). (**C**,**D**) Coronal sections of the brain as indicated in A and B. RGC axons targeted to the lateral geniculate nucleus normally in both genotypes. (**E**,**F**) CTB-488 was injected into the right eyes to visualize RGC axon targeting in the superior colliculus (SC) in *Atoh7*$^{+/G}$ (E) and *Atoh7*$^{G/G}$:*Neurod1*$^{Atoh7/Atoh7}$ (F) brains. CTB-488 is evenly distributed in the SC of the *Atoh7*$^{+/G}$ brain (E), but slightly towards the anterior SC of the *Atoh7*$^{G/G}$:*Neurod1*$^{Atoh7/Atoh7}$ brain (F).

LGN of the thalamus is the gateway that relays visual pathways to the primary visual cortex, and the SC is a midbrain structure involved in the generation of visual guided saccadic movement. To determine whether *Neurod1*^{Atoh7}-induced RGCs projected to the LGN, we traced RGC axons by injecting CTB-594 into the eyes of both wild-type and *Atoh7*$^{G/G}$:*Neurod1*$^{Atoh7HA/Atoh7HA}$ mice. Coronal sections showed that RGC axons in both wild-type and *Atoh7*$^{G/G}$:*Neurod1*$^{Atoh7HA/Atoh7HA}$ mice projected normally across the optical chiasm (Fig. 6A,B) to dorsal and ventral LGN (Fig. 6C,D).

The retinocollicular projection establishes a topographic map between RGCs and the SC. RGCs along the dorsal-ventral (D-V) axis topographically project to the medial-lateral (M-L) axis of the SC, whereas RGCs along nasal-temporal (N-L) axis topographically project to the posterior-anterior (P-A) axis of the SC. Tracing *Neurod1*^{Atoh7}-induced RGC axon projections with CTB-488 showed that while wild-type and *Neurod1*$^{Atoh7HA3/Atoh7HA3}$ RGC axons occupied the entire SC, as viewed by the filled fluorescent dye in the SC (Fig. 6E), RGC axons of *Atoh7*$^{G/G}$:*Neurod1*$^{Atoh7HA3/Atoh7HA3}$ mice projected to slightly more anterior areas in the SC.

Atoh7$^{G/G}$:*Neurod1*$^{Atoh7/Atoh7}$ RGCs partially rescue defective electroretinogram (ERG) signals in *Atoh7*$^{G/G}$ retinas

Because the *Atoh7*$^{G/G}$:*Neurod1*$^{Atoh7/Atoh7}$ mice partially restore the optic nerves through which RGC axons project to the major regions in the brain, we also expected some restoration of electroretinogram (ERG) responses in *Atoh7*$^{G/G}$:*Neurod1*^{Atoh7Atoh7} mice. Representative dark-adapted ERG responses to flashes of increasing stimulus strengths for four genotypes tested are shown in Fig. 7A. In control *Atoh7*$^{+/G}$ mice (Fig. 7A), the dark-adapted ERG in response to a weak stimulus, e.g. –4.7 log sc td-s, is dominated by two signals from inner retina: positive (p) and negative (n) scotopic response (Saszik et al., 2002). Generation of the positive STR requires that RGCs are functional, the negative STR also relies on RGC function, but the extent varies (Moshiri et al., 2008; Alarcón-Martínez et al., 2010). *Atoh7*$^{G/G}$ mice (Fig. 7A) hardly showed either of the waves originating from inner retina that were present in the ERG of the *Atoh7*$^{+/G}$ mice. The small positive wave that was present for the –4.7 log sc td-s stimulus was either residual pSTR, or the most sensitive part of the b-wave, which is generated by responses of ON (rod-driven) bipolar cells in the scotopic ERG (Robson and Frishman, 1995, Robson et al., 2004). Similar results have been reported previously, although in one study, a nSTR was still present in the *Atoh7*$^{-/-}$ mice (Moshiri et al., 2008, Brzezinski et al., 2005).

The ERG responses to the weakest stimuli in *Atoh7*$^{G/G}$:*Neurod1*$^{Atoh7/Atoh7}$ mice were similar in waveform, but smaller than the responses of *Atoh7*$^{+/G}$ mice (Fig. 7A), indicating the presence of more RGC function than in the *Atoh7*$^{G/G}$ mice. Recordings from one *Atoh7*$^{G/G}$:*Neurod1*$^{Atoh7/+}$ (not illustrated) were very similar to those for the *Atoh7*$^{G/G}$:*Neurod1*$^{Atoh7/Atoh7}$ group.

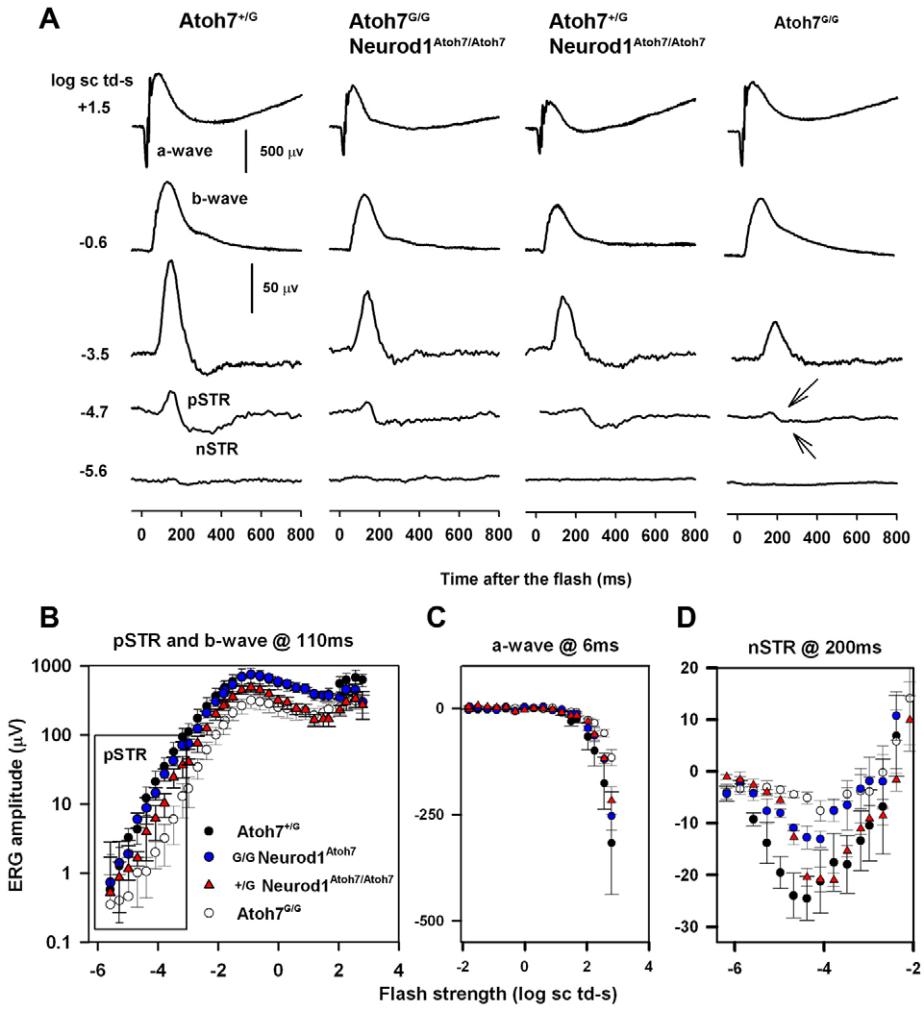

Fig. 7. ERG analysis. (**A**) Scotopic full-field ERG responses to brief flashes recorded from one mouse from each of the four genotypes. Stimulus strength increases from bottom to top. Arrows in the right column indicated missing STRs in this animal. (**B-D**) Stimulus versus ERG amplitude plots measured at fixed time after the brief stimulus flash for the four genotypes: *Atoh7*$^{+/G}$ (*n*=4), *Atoh7*$^{G/G}$*:Neurod1*$^{Atoh7/+}$ (*n*=3), *Atoh7*$^{+/G}$*:Neurod1*$^{Atoh7/Atoh7}$ and *Atoh7*$^{G/G}$ (*n*=3). (B) pSTR and b-wave amplitudes at 110 ms, (C) nSTR amplitudes at 200 ms and (D) a-wave amplitudes at 6 ms after the flash. The error bars are standard errors.

Finally, *Atoh7*$^{+/G}$*:Neurod1*$^{Atoh7/Atoh7}$ (Fig. 7A) also showed more evidence of inner retinal activity than did *Atoh7*$^{G/G}$ mice, particularly for the nSTR. In all four groups, the ERGs to stronger stimuli included common features of the flash ERG; b-waves that increased in amplitude with stimulus strength, and for the strongest stimuli, e.g. 2.1 log sc td s, a negative-going a-wave, which reflects photoreceptor currents (Robson et al., 2004; Hood and Birch, 1990; Jamison et al., 2001), was present at the beginning of the response. However, further analysis showed that b-waves were consistently smaller than control *Atoh7*$^{+/G}$ b-waves, in certain groups.

In order to quantify comparisons of the ERGs of mice in the four different groups, stimulus versus ERG amplitude plots were constructed based on measurements at peak times of the ERG waves. Plots are shown for pSTR and b-wave measured at 110 ms after the flash (Fig. 7B) and for nSTR measured at 200 ms at the trough of the response (Fig. 7C). Fig. 7D shows the amplitude measured at 6 ms after the flash on the leading edge of the a-wave. As predicted by the ERG traces (Fig. 7A), and documented in supplementary material Table S1, pSTR amplitudes were significantly lower in the Atoh7-null mice than in the *Atoh7*$^{+/G}$ controls and in the *Atoh7*$^{G/G}$*:Neurod1*$^{Atoh7/+}$ group. For the pSTR, ERG amplitudes for the different groups were compared only in the region of the box in the pSTR/b-wave plot. The nSTR in *Atoh7*-null mice was significantly lower than in *Atoh7*$^{+/G}$ control as expected, but also the *Atoh7*$^{G/G}$*:Neurod1*$^{Atoh7/Atoh7}$ group. STRs of *Atoh7*$^{G/G}$*:Neurod1*$^{Atoh7/+}$ and *Atoh7*$^{+/G}$*:Neurod1*$^{Atoh7/Atoh7}$ were not significantly different from one another. A-wave amplitudes were not significantly different across groups, but b-wave amplitudes measured at 110 ms were significantly lower in *Atoh7*$^{G/G}$ than in either *Atoh7*$^{+/G}$ and *Atoh7*$^{G/G}$*:Neurod1*$^{Atoh7/+}$ groups. B-wave amplitudes were also measured from a-wave trough to b-wave peak, which is a more traditional measure that is independent of timing of waves. The two b-wave measures yielded very similar results, as shown in supplementary material Table S1. Plots of trough-to-peak amplitudes were not included in Fig. 7. Although b-wave amplitudes of *Atoh7*$^{G/G}$*:Neurod1*$^{Atoh7/+}$ were not significantly larger in amplitude than *Atoh7*$^{G/G}$, they were significantly lower than in the *Atoh7*$^{+/G}$ control mice (supplementary material Table S1). In summary, the *Atoh7*$^{G/G}$*:Neurod1*$^{Atoh7/+}$ group showed restoration of pSTR, which relies ganglion cell integrity, and b-wave, which relies on bipolar cell function. Consistent with morphological findings, the improvement in positive going potentials did not occur at a significant level for the *Atoh7*$^{+/G}$*:Neurod1*$^{Atoh7/Atoh7}$ mice. By contrast, for the nSTR, amplitude was significant larger in the *Atoh7*$^{+/G}$*:Neurod1*$^{Atoh7/Atoh7}$ mice than in the than in *Atoh7*$^{G/G}$ mice, but this did not occur for the *Atoh7*$^{G/G}$*:Neurod1*$^{Atoh7/+}$ group, in which the nSTR amplitude was improved, but not significantly. The nSTR relies on amacrine as well as ganglion cell function in mice, and is mediated via glial cell currents. Interestingly, Fig. 7D shows that nSTR in the *Atoh7*$^{+/G}$*:Neurod1*$^{Atoh7/Atoh7}$ mice, as in the *Atoh7*$^{G/G}$ mice, was not present at the lowest stimulus strengths,

and only emerged for a stimulus almost a log unit stronger where the *Atoh7*$^{+/G}$ control response was nearly maximal.

Differential *in vivo* use of an Atoh7-mediated enhancer by Atonal-like factors

Atoh7 and Neurod1 both belong to Atonal-like transcription factor family. They form heterodimer with E12/E47 factors that selectively bind to specific E-box sequences, including CAGGTG, CAGCTG, CAGATG, CATATG and CATGTG, to activate a distinct set of downstream genes (De Masi et al., 2011). Based on current knowledge, we cannot predict whether any specific domain within Atoh7 or Neurod1 sequences can discriminate one from the other to determine their *in vivo* target specificity. The results presented by Mao et al. (Mao et al., 2008b) demonstrated that Neurod1 functions in *Atoh7*-expressing RPCs to activate RGC genes. This raises the issue of why Neurod1 cannot activate RGC genes in *Neurod1*-expressing RPCs. Conversely, as we showed above, Atoh7 converts *Neurod1*-expressing RPCs to RGC-competent RPCs.

To begin to understand the *in vivo* target specificity of Atoh7 and Neurod1, we performed chromatin immunoprecipitation coupled with parallel sequencing (ChIP-Seq) to uncover genome-wide DNA-binding sites for Atoh7. We used E14.5 *Atoh7*$^{HA/HA}$ retinas to prepare fragmented chromatin, performed ChIP-Seq on the DNA fragments with an anti-HA antibody using wild-type retinas as control, and identified ~1500 *in vivo* targets of Atoh7 (C.-A.M., Yue Lu, W.H.K. and Shoudan Liang, unpublished). One of the strongest peaks in the data analysis was within the Neurexin III (*Nrxn3*) locus. *Nrxn3* encodes a neuron-specific cell-surface molecule and is widely expressed in developing central nervous system, including the retina (Püschel and Betz, 1995). The *Nrxn3* Atoh7-binding peak encompassed a 326 bp evolutionarily conserved sequence mapping to chr12:90280146-90280471, which lies within intron 3 of *Nrxn3* (Fig. 8A,B).

Five E-boxes were found in this region (supplementary material Fig. S2), all belonging to the predicted Atoh7-binding E-box sequences. Most notably, two consecutive E-box elements were clustered in the middle of this peak (supplementary material Fig. S2). To confirm whether Atoh7 binds to this element *in vivo*, we performed qPCR on the immunoprecipitated DNA fragment from E14.5 *Atoh7*$^{HA/HA}$ retinas. A 16-fold enrichment of occupancy in this region was observed compared with non-specific occupancy by anti-HA antibody on E14.5 wild-type retina (Fig. 8C). Weaker but detectable occupancy of Atoh7 in this region was also found in *Neurod1*$^{Atoh7/Atoh7}$ retinas (Fig. 8C). In addition, we detected a weak, but reproducible, occupancy of Atoh7 in a region near *Tbr1*, which is expressed in a small subset of RGCs (Mao et al., 2008a). By contrast, we did not detect any *in vivo* occupancy of Neurod1 in this region in the retina, although a weak occupancy of Neurod1 in the same region in E14.5 brain tissue was detected (data not shown).

Nrxn3 was expressed largely in the developing ganglion cell layer of E14.5 retinas (Fig. 8D). However, in the absence of *Atoh7*, *Nrxn3* expression was downregulated by ~41% (Fig. 8E,F), indicating that its expression was dependent on *Atoh7* but not on *Neurod1* in the developing retina. These results suggested that the *Nrxn3* element is a direct target of Atoh7, and the expression of *Nrxn3* depends on *Atoh7*. The results additionally support the notion that there is a differential use of the *Nrxn3* element by Atoh7 and Neurod1 in different regions of the developing central nervous system.

DNA-binding elements identified by ChIP-Seq analysis often function as enhancers, which can be tested as such in the appropriate experimental context (Visel et al., 2009). To test whether this region in *Nrxn3* confers Atoh7-mediated enhancer activity, we generated two transgenic mouse lines carrying the *Nrxn3*^{A7E}*-HSP68lacZ* construct (Fig. 9A), and bred them to *Atoh7*$^{HA/HA}$ mice to produce *Atoh7*$^{HA/HA}$*; Nrxn3*^{A7E}*-HSP68LacZ* retinas. We compared the expression profile of Atoh7-HA and *lacZ* in E14.5 retinas by co-immunostaining and found that ~70% of Atoh7HA-expressing cells also expressed *lacZ*, suggesting this sequence functions as a bona fide Atoh7 enhancer (Fig. 9B-D). Surprisingly, many *lacZ*-positive RPCs were found clustered in area where presumptive photoreceptors reside. We then compared the co-expression of *lacZ* and *Neurod1* and found that many *lacZ*-positive RPCs expressed *Neurod1* (Fig. 9E-G). This result was unexpected, as endogenous *Nrxn3* is not expressed in the region for photoreceptor progenitors and the *Nrxn3*^{A7E} element was not bound *in vivo* by Neurod1. Additionally, another *Atonal*-related bHLH factor Ngn2 (Hufnagel et al., 2010) was also expressed in *lacZ*-positive RPCs (Fig. 9H-J). Taken together, our results suggested that *Nrxn3*^{A7E} was bound and used *in vivo* by Atoh7, and likely functioned as an enhancer for *Nrxn3* expression *in vivo*. It also suggested that,

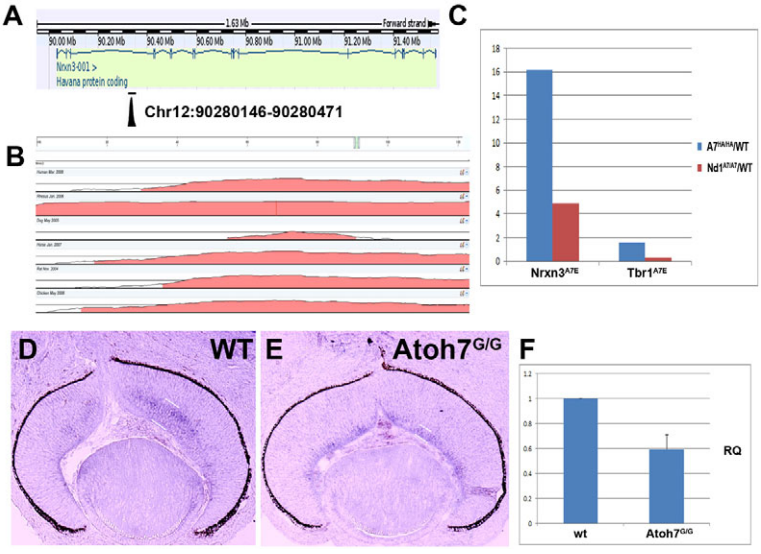

Fig. 8. Atoh7 binds to intron 3 of *Nrxn3* and regulates *Nrxn3* expression. (**A**) The sequence peak for *in vivo* Atoh7 occupancy in E14.5 retinal DNA was uncovered in intron 3 of *Nrxn3* by ChiP-Seq. (**B**) Whole-genome comparative analysis using Vista Point (http://pipeline.lbl.gov/cgi-bin/gateway2?selector=vistapoint) reveals that the Nrxn3^{A7E} peak sequence (chr12:90280146-90280471) is evolutionarily conserved among multiple vertebrate species. (**C**) Quantitative PCR analysis of Nrxn3^{A7E} and Tbr1^{A7E} peaks in *Atoh7*$^{HA/HA}$ and *Neurod1*$^{Atoh7HA/Atoh7HA}$ retinas using wild-type retinas as a baseline. (**D**,**E**) Expression of *Nrxn3* (signal between white lines) in E14.5 wild-type (D) and *Atoh7*$^{G/G}$ (E) retinas. (**F**) Quantitative RT-PCR analysis of *Nrxn3* expression in E14 wild-type and Atoh7$^{G/G}$ retinas. RQ indicates relative quantification of *Nrxn3* expression in E14.5 wild-type (wt) and Atoh7$^{G/G}$ retinas using *GAPDH* expression as an internal control.

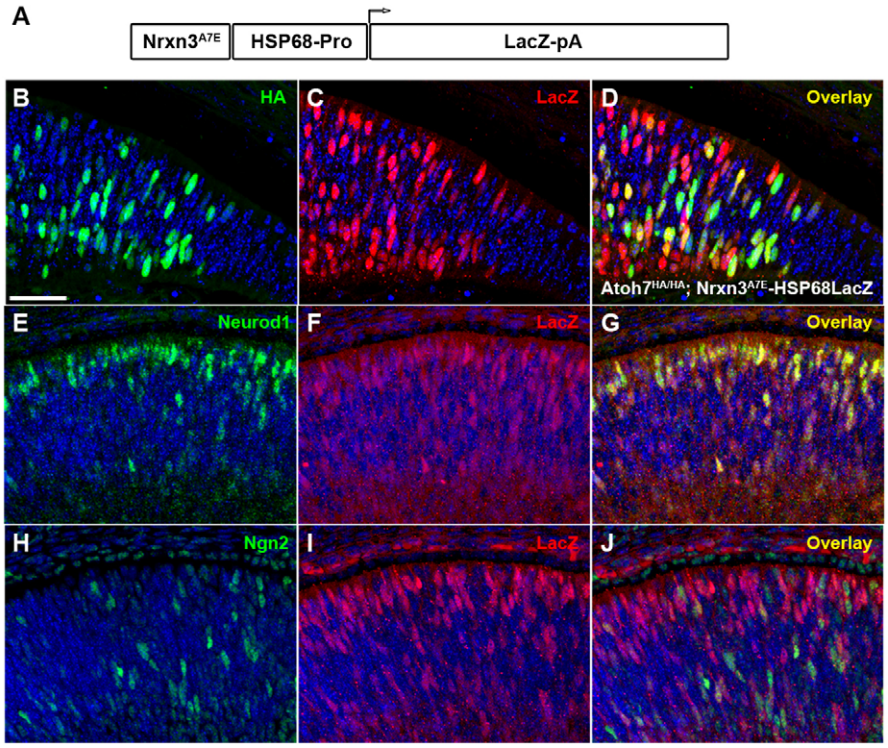

Fig. 9. *Nrxn3^{A7E}* peak sequence functions as an *in vivo* enhancer for *Atonal*-class bHLH factors. (**A**) *Nrxn3^{A7E}* peak sequence was linked to a *HSP68-LacZ-pA* construct to generate transgenic lines for enhancer analysis. (**B-D**) Co-expression of Atoh7HA and *lacZ* in E14.5 *Atoh7$^{HA/HA}$:Nrxn3^{A7E}HSP68LacZ*-pA retinal sections. (**E-G**) Co-expression of Neurod1 and *lacZ*. (**H-J**) Co-expression of Ngn2 and *lacZ*. Scale bar: 40 μm.

when this enhancer element was placed in a different context, it could be recognized and used by other related bHLH factors that were otherwise selectively prohibited.

DISCUSSION

In a previous study, we replaced *Atoh7* with *Neurod1* and found that, in *Atoh7$^{Neurod1/Neurod1}$* retinas, *Atoh7*-expressing RPCs are pre-programmed to produce RGCs provided that the bHLH proneural gene *Atoh7* or *Neurod1* is present (Mao et al., 2008b). In the present study, we addressed how *Neurod1*-expressing RPCs would respond to the replacement of *Neurod1* with *Atoh7*. Our results demonstrate that *Atoh7* acts dominantly in *Neurod1*-expressing RPCs to activate the RGC genetic program. In the absence of endogenous *Atoh7*, *Neurod1^{Atoh7}* directed RPCs to specify an RGC fate, differentiate into RGCs, form an optic nerve, make proper axon projections to brain and produce an ERG response. These data support the idea that *Atoh7* acts as a 'master regulator' for establishing an RGC competency state in non-*Atoh7*-expressing RPCs. By contrast, *Neurod1* does not possess this activity in the same population of RPCs. In *Atoh7*-expressing RPCs, *Neurod1* adapts to the new environment and acts like *Atoh7* to establish RGC competence state. Two major conclusions can be drawn from these consecutive studies. The first is that the intrinsic program in *Atoh7*-expressing RPCs redirects the function of *Neurod1* to act as *Atoh7* in RGC formation, whereas *Neurod1*-expressing RPCs have sufficient plasticity to be reprogrammed by *Atoh7*. Second, *Atoh7* functions as a dominant factor to convert other RPCs into RGC competence state, whereas *Neurod1* does not. The most challenging question arising from our studies is why *Atoh7*-expressing RPCs are distinct from *Neurod1*-expressing RPCs, especially as RPCs are thought to be flexible in selecting their final cell fate (Gomes et al., 2011). *Neurod1* cannot activate the RGC genetic program in its endogenous environment, yet it can do so in *Atoh7*-expressing RPCs. What distinguishes *Atoh7*-expressing RPCs from *Neurod1*-expressing RPCs and *Atoh7* from *Neurod1*?

One possible explanation is that the expression levels of *Atoh7* and *Neurod1* in the two RPC subpopulations govern whether RGC genes are activated. Our results indicate that on a per cell basis, *Atoh7* expression in *Neurod1$^{Atoh7/Atoh7}$* retinas is 10% of the levels in wild-type embryos. This suggests that a threshold level of *Atoh7* is involved in specifying RPCs towards an RGC fate. Perhaps *Neurod1* expression in *Atoh7$^{Neurod1/Neurod1}$* retinas achieves this threshold in *Atoh7*-expressing RPCs, although not fully. However, *Neurod1* may fail to reach the necessary threshold level to activate RGC genes in *Neurod1*-expressing RPCs. It is possible that overexpressing *Neurod1* in *Neurod1*-expressing RPCs may enhance RGC differentiation, but the appropriate animal study is presently not feasible. Similar to the notion of dose effect, the expression level of *Atoh7* has also been implicated to regulate the initial RGC number in RGC specification process (Prasov et al., 2012).

Another possibility is that *Atoh7* and *Neurod1* selectively activate distinct sets of downstream genes. For Atoh7, Neurod1 and other bHLH factors to function precisely in their respective RPCs, each needs to coordinate with chromatin remodeling factors to generate suitable local chromatin structures and histone marks to trigger the activation of the gene. In our pilot ChiP-Seq assay for Atoh7 *in vivo* targets, we identified *Nrxn3* as an Atoh7 target gene and found that whereas Atoh7 binds to the presumptive enhancer in intron 3, Neurod1 does not occupy this region in retina. Notably, in the developing brain, where *Neurod1* and *Nrxn3* expression patterns partially overlap, we readily detected Neurod1 occupancy in the same genomic region of *Nrnx3*. Furthermore, a transgene reporter driven by the intron 3 enhancer faithfully reports Atoh7 activity in retina. Additionally, other bHLH factors such as Neurod1 and Ngn2, appeared to activate the intron 3 enhancer in the retina, whereas in normal development, *Nrxn3* expression does not rely on these factors. These results suggest that related bHLH factors have the inherent capability of activating gene expression at enhancers that are normally inaccessible to them.

Post-translational modification of bHLH factors may also be involved in establishing target gene specificity among related bHLH factors. For example, a GSKβ-insensitive form of *Xneurod1* was shown to convey RGC fate in frog retinas, implying an interaction between Neurod1 and the Wnt/β-catenin pathway (Moore et al., 2002). Post-translational modification of key transcriptional regulators, such as Nrl and Vax2, has recently been realized as another layer of regulation of cell fate determination during retinogenesis (Roger et al., 2010; Kim and Lemke, 2006; Onishi et al., 2010). Future studies with purified *Atoh7*- and *Neurod1*-expressing RPCs may aid in distinguishing the different molecular contents in each RPC subpopulation.

The establishment of RGC competency requires coordinated integration of the Atoh7-dependent intrinsic program with the dynamic local environmental signals. It was recently discovered that linage-specific regulators can direct the Bmp and Wnt signaling effectors Smad and TCF7 to lineage-specific target genes to control the genetic program defining cellular identity (Mullen et al., 2011, Trompouki et al., 2011). It is possible that this type of dominant mechanism is also being used by Atoh7 in a similar way to convey RGC competency. In the ChiP-Seq dataset for Atoh7, we found that the majority of Atoh7 target genes fall into two functional categories, those involved in transcriptional regulation, and those involved in axonal guidance (C.A.-M. and W.H.K., unpublished). The *Atoh7* gene targets that encode transcriptional regulators most probably play a role in regulating the downstream cascade of events for RGC differentiation. What was perhaps less expected was the identification of many Atoh7 gene targets involved in axonal guidance. When RGCs are first generated in embryonic retinas they are located close to the optic nerve head (Oster et al., 2004). One of the first events of nascent RGCs is to detach their ventricular processes to form an unipolar RGC, and their vitreal processes transformed into an axon growth cone (Hinds and Hinds, 1974; Oster et al., 2004). The earliest born RGCs are considered pioneer neurons, which serve as platform for later-born RGC axons (Raper and Mason, 2010). Consistent with our ChIP-Seq results, a recent study has implied that Atoh7 plays a role in activating pioneer neurons (Brzezinski et al., 2012). *Atoh7*-expressing RPCs were known to give rise to RGC and photoreceptor lineages (Yang et al., 2003). Loss of *Atoh7* led to increased production of cone photoreceptors (Brown et al., 2001). These data together suggest that some RGCs and cones share the same *Atoh7*-expressing RPCs during retinogenesis, and the absence of *Atoh7* provides a permissive environment to allow fate shifting to cones. However, the likely permissive effect of the absence of M-cones in *Neurod1*$^{Atoh7/Atoh7}$ RPCs on the induction of RGC fates and the molecular mechanisms underlying the differential in vivo target selection between similar bHLH factors are presently unresolved.

Acknowledgements
We thank the internal Genetically Engineered Mouse Facility for generating mouse lines, the DNA Analysis Facility for DNA sequencing and ChiP-Seq, and the High Resolution Electron Microscopy Facility for TEM. We thank Drs Yue Lu and Shoudan Liang in the Department of Bioinformatics and Computational Biology for analyzing the initial ChiP-Seq dataset and revealing Nrxn3^{A7E} element.

Funding
These core facilities are supported in part by a NCI Cancer Center Core Grant [CA016672]. The work was supported by grants from the National Eye Institute to W.H.K. [EY011930 and EY010608-139005] and to L.J.F. [EY06671], and by the Robert A. Welch Foundation [G-0010 to W.H.K.]. Deposited in PMC for release after 12 months.

Competing interests statement
The authors declare no competing financial interests.

Supplementary material
Supplementary material available online at
http://dev.biologists.org/lookup/suppl/doi:10.1242/dev.085886/-/DC1

References
Agathocleous, M. and Harris, W. A. (2009). From progenitors to differentiated cells in the vertebrate retina. *Annu. Rev. Cell Dev. Biol.* **25**, 45-69.
Akagi, T., Inoue, T., Miyoshi, G., Bessho, Y., Takahashi, M., Lee, J. E., Guillemot, F. and Kageyama, R. (2004). Requirement of multiple basic helix-loop-helix genes for retinal neuronal subtype specification. *J. Biol. Chem.* **279**, 28492-28498.
Alarcón-Martínez, L., Avilés-Trigueros, M., Galindo-Romero, C., Valiente-Soriano, J., Agudo-Barriuso, M., Villa, P. L., Villegas-Pérez, M. P. and Vidal-Sanz, M. (2010). ERG changes in albino and pigmented mice after optic nerve transection. *Vision Res.* **50**, 2176-2187.
Brown, N. L., Kanekar, S., Vetter, M. L., Tucker, P. K., Gemza, D. L. and Glaser, T. (1998). Math5 encodes a murine basic helix-loop-helix transcription factor expressed during early stages of retinal neurogenesis. *Development* **125**, 4821-4833.
Brown, N. L., Patel, S., Brzezinski, J. and Glaser, T. (2001). Math5 is required for retinal ganglion cell and optic nerve formation. *Development* **128**, 2497-2508.
Brzezinski, J. A., 4th, Brown, N. L., Tanikawa, A., Bush, R. A., Sieving, P. A., Vitaterna, M. H., Takahashi, J. S. and Glaser, T. (2005). Loss of circadian photoentrainment and abnormal retinal electrophysiology in Math5 mutant mice. *Invest. Ophthalmol. Vis. Sci.* **46**, 2540-2551.
Brzezinski, J. A., 4th, Prasov, L. and Glaser, T. (2012). Math5 defines the ganglion cell competence state in a subpopulation of retinal progenitor cells exiting the cell cycle. *Dev. Biol.* **365**, 395-413.
Cherry, T. J., Wang, S., Bormuth, I., Schwab, M., Olson, J. and Cepko, C. L. (2011). NeuroD factors regulate cell fate and neurite stratification in the developing retina. *J. Neurosci.* **31**, 7365-7379.
De Masi, F., Grove, C. A., Vedenko, A., Alibés, A., Gisselbrecht, S. S., Serrano, L., Bulyk, M. L. and Walhout, A. J. (2011). Using a structural and logics systems approach to infer bHLH-DNA binding specificity determinants. *Nucleic Acids Res.* **39**, 4553-4563.
Elshatory, Y., Deng, M., Xie, X. and Gan, L. (2007). Expression of the LIM-homeodomain protein Isl1 in the developing and mature mouse retina. *J. Comp. Neurol.* **503**, 182-197.
Feng, L., Xie, X., Joshi, P. S., Yang, Z., Shibasaki, K., Chow, R. L. and Gan, L. (2006). Requirement for Bhlhb5 in the specification of amacrine and cone bipolar subtypes in mouse retina. *Development* **133**, 4815-4825.
Fu, X., Kiyama, T., Li, R., Russell, M., Klein, W. H. and Mu, X. (2009). Epitope-tagging Math5 and Pou4f2: new tools to study retinal ganglion cell development in the mouse. *Dev. Dyn.* **238**, 2309-2317.
Fujitani, Y., Fujitani, S., Luo, H., Qiu, F., Burlison, J., Long, Q., Kawaguchi, Y., Edlund, H., MacDonald, R. J., Furukawa, T. et al. (2006). Ptf1a determines horizontal and amacrine cell fates during mouse retinal development. *Development* **133**, 4439-4450.
Gan, L., Wang, S. W., Huang, Z. and Klein, W. H. (1999). POU domain factor Brn-3b is essential for retinal ganglion cell differentiation and survival but not for initial cell fate specification. *Dev. Biol.* **210**, 469-480.
Ghiasvand, N. M., Rudolph, D. D., Mashayekhi, M., Brzezinski, J. A., 4th, Goldman, D. and Glaser, T. (2011). Deletion of a remote enhancer near ATOH7 disrupts retinal neurogenesis, causing NCRNA disease. *Nat. Neurosci.* **14**, 578-586.
Gomes, F. L., Zhang, G., Carbonell, F., Correa, J. A., Harris, W. A., Simons, B. D. and Cayouette, M. (2011). Reconstruction of rat retinal progenitor cell lineages in vitro reveals a surprising degree of stochasticity in cell fate decisions. *Development* **138**, 227-235.
Hatakeyama, J. and Kageyama, R. (2004). Retinal cell fate determination and bHLH factors. *Semin. Cell Dev. Biol.* **15**, 83-89.
Hinds, J. W. and Hinds, P. L. (1974). Early ganglion cell differentiation in the mouse retina: an electron microscopic analysis utilizing serial sections. *Dev. Biol.* **37**, 381-416.
Hood, D. C. and Birch, D. G. (1990). A quantitative measure of the electrical activity of human rod photoreceptors using electroretinography. *Vis. Neurosci.* **5**, 379-387.
Hufnagel, R. B., Le, T. T., Riesenberg, A. L. and Brown, N. L. (2010). Neurog2 controls the leading edge of neurogenesis in the mammalian retina. *Dev. Biol.* **340**, 490-503.
Inoue, T., Hojo, M., Bessho, Y., Tano, Y., Lee, J. E. and Kageyama, R. (2002). Math3 and NeuroD regulate amacrine cell fate specification in the retina. *Development* **129**, 831-842.

Jamison, J. A., Bush, R. A., Lei, B. and Sieving, P. A. (2001). Characterization of the rod photoresponse isolated from the dark-adapted primate ERG. *Vis. Neurosci.* **18**, 445-455.
Kay, J. N., Voinescu, P. E., Chu, M. W. and Sanes, J. R. (2011). Neurod6 expression defines new retinal amacrine cell subtypes and regulates their fate. *Nat. Neurosci.* **14**, 965-972.
Kim, J. W. and Lemke, G. (2006). Hedgehog-regulated localization of Vax2 controls eye development. *Genes Dev.* **20**, 2833-2847.
Kothary, R., Clapoff, S., Darling, S., Perry, M. D., Moran, L. A. and Rossant, J. (1989). Inducible expression of an hsp68-lacZ hybrid gene in transgenic mice. *Development* **105**, 707-714.
Le, T. T., Wroblewski, E., Patel, S., Riesenberg, A. N. and Brown, N. L. (2006). Math5 is required for both early retinal neuron differentiation and cell cycle progression. *Dev. Biol.* **295**, 764-778.
Liu, M., Pereira, F. A., Price, S. D., Chu, M.-J., Shope, C., Himes, D., Eatock, R. A., Brownell, W. E., Lysakowski, A. and Tsai, M. J. (2000). Essential role of BETA2/NeuroD1 in development of the vestibular and auditory systems. *Genes Dev.* **14**, 2839-2854.
Liu, H., Etter, P., Hayes, S., Jones, I., Nelson, B., Hartman, B., Forrest, D. and Reh, T. A. (2008). NeuroD1 regulates expression of thyroid hormone receptor 2 and cone opsins in the developing mouse retina. *J. Neurosci.* **28**, 749-756.
Livesey, F. J. and Cepko, C. L. (2001). Vertebrate neural cell-fate determination: lessons from the retina. *Nat. Rev. Neurosci.* **2**, 109-118.
Mao, C. A., Kiyama, T., Pan, P., Furuta, Y., Hadjantonakis, A. K. and Klein, W. H. (2008a). Eomesodermin, a target gene of Pou4f2, is required for retinal ganglion cell and optic nerve development in the mouse. *Development* **135**, 271-280.
Mao, C. A., Wang, S. W., Pan, P. and Klein, W. H. (2008b). Rewiring the retinal ganglion cell gene regulatory network: Neurod1 promotes retinal ganglion cell fate in the absence of Math5. *Development* **135**, 3379-3388.
Moore, K. B., Schneider, M. L. and Vetter, M. L. (2002). Posttranslational mechanisms control the timing of bHLH function and regulate retinal cell fate. *Neuron* **34**, 183-195.
Moshiri, A., Gonzalez, E., Tagawa, K., Maeda, H., Wang, M., Frishman, L. J. and Wang, S. W. (2008). Near complete loss of retinal ganglion cells in the math5/brn3b double knockout elicits severe reductions of other cell types during retinal development. *Dev. Biol.* **316**, 214-227.
Mu, X., Fu, X., Beremand, P. D., Thomas, T. L. and Klein, W. H. (2008). Gene regulation logic in retinal ganglion cell development: Isl1 defines a critical branch distinct from but overlapping with Pou4f2. *Proc. Natl. Acad. Sci. USA* **105**, 6942-6947.
Mullen, A. C., Orlando, D. A., Newman, J. J., Lovén, J., Kumar, R. M., Bilodeau, S., Reddy, J., Guenther, M. G., DeKoter, R. P. and Young, R. A. (2011). Master transcription factors determine cell-type-specific responses to TGF-β signaling. *Cell* **147**, 565-576.
Ohsawa, R. and Kageyama, R. (2008). Regulation of retinal cell fate specification by multiple transcription factors. *Brain Res.* **1192**, 90-98.
Onishi, A., Peng, G. H., Chen, S. and Blackshaw, S. (2010). Pias3-dependent SUMOylation controls mammalian cone photoreceptor differentiation. *Nat. Neurosci.* **13**, 1059-1065.
Oster, S. F., Deiner, M., Birgbauer, E. and Sretavan, D. W. (2004). Ganglion cell axon pathfinding in the retina and optic nerve. *Semin. Cell Dev. Biol.* **15**, 125-136.
Pennesi, M. E., Cho, J. H., Yang, Z., Wu, S. H., Zhang, J., Wu, S. M. and Tsai, M. J. (2003). BETA2/NeuroD1 null mice: a new model for transcription factor-dependent photoreceptor degeneration. *J. Neurosci.* **23**, 453-461.
Perron, M. and Harris, W. A. (2000). Determination of vertebrate retinal progenitor cell fate by the Notch pathway and basic helix-loop-helix transcription factors. *Cell. Mol. Life Sci.* **57**, 215-223.
Prasov, L., Nagy, M., Rudolph, D. D. and Glaser, T. (2012). Math5 (Atoh7) gene dosage limits retinal ganglion cell genesis. *Neuroreport* **23**, 631-634.
Püschel, A. W. and Betz, H. (1995). Neurexins are differentially expressed in the embryonic nervous system of mice. *J. Neurosci.* **15**, 2849-2856.
Raper, J. and Mason, C. (2010). Cellular strategies of axonal pathfinding. *Cold Spring Harb. Perspect. Biol.* **2**, a001933.
Robson, J. G. and Frishman, L. J. (1995). Response linearity and kinetics of the cat retina: the bipolar cell component of the dark-adapted electroretinogram. *Vis. Neurosci.* **12**, 837-850.
Robson, J. G., Maeda, H., Saszik, S. M. and Frishman, L. J. (2004). In vivo studies of signaling in rod pathways of the mouse using the electroretinogram. *Vision Res.* **44**, 3253-3268.
Rodieck, R. W. (1998). *The First Steps in Seeing.* Sunderland, MA: Sinauer Associates.
Roger, J. E., Nellissery, J., Kim, D. S. and Swaroop, A. (2010). Sumoylation of bZIP transcription factor NRL modulates target gene expression during photoreceptor differentiation. *J. Biol. Chem.* **285**, 25637-25644.
Saszik, S. M., Robson, J. G. and Frishman, L. J. (2002). The scotopic threshold response of the dark-adapted electroretinogram of the mouse. *J. Physiol.* **543**, 899-916.
Trimarchi J. M., Stadler M. B. and Cepko C. L. (2008). Individual retinal progenitor cells display extensive heterogeneity of gene expression. *PLoS ONE* **3,** e1588.
Trompouki, E., Bowman, T. V., Lawton, L. N., Fan, Z. P., Wu, D. C., DiBiase, A., Martin, C. S., Cech, J. N., Sessa, A. K., Leblanc, J. L. et al. (2011). Lineage regulators direct BMP and Wnt pathways to cell-specific programs during differentiation and regeneration. *Cell* **147**, 577-589.
Tsai, W. W., Wang, Z., Yiu, T. T., Akdemir, K. C., Xia, W., Winter, S., Tsai, C. Y., Shi, X., Schwarzer, D., Plunkett, W. et al. (2010). TRIM24 links a non-canonical histone signature to breast cancer. *Nature* **468**, 927-932.
Vetter, M. L. and Brown, N. L. (2001). The role of basic helix-loop-helix genes in vertebrate retinogenesis. *Semin. Cell Dev. Biol.* **12**, 491-498.
Visel, A., Blow, M. J., Li, Z., Zhang, T., Akiyama, J. A., Holt, A., Plajzer-Frick, I., Shoukry, M., Wright, C., Chen, F. et al. (2009). ChIP-seq accurately predicts tissue-specific activity of enhancers. *Nature* **457**, 854-858.
Wallace, V. A. (2011). Making a retina – from the building blocks to clinical application. *Stem Cells* **29**, 412-417.
Wang, S. W., Kim, B. S., Ding, K., Wang, H., Sun, D., Johnson, R. L., Klein, W. H. and Gan, L. (2001). Requirement for math5 in the development of retinal ganglion cells. *Genes Dev.* **15**, 24-29.
Yang, Z., Ding, K., Pan, L., Deng, M. and Gan, L. (2003). Math5 determines the competence state of retinal ganglion cell progenitors. *Dev. Biol.* **264**, 240-254.